Motion compensation in ISAR imaging using the registration-restoration-fusion approach

Thayananthan Thayaparan, George Lampropoulos, LJubiša Stanković

Abstract—**The distortion in the ISAR image of a target is a result of small time-varying perturbed motion experienced by the target during the image integration period and is attributed to a phase modulation effect of the radar return from the target. Large distortion in ISAR images of a moving target has been investigated and demonstrated under controlled experiments and simulation. Results from the analysis suggest that severe distortion is attributed to the phase modulation effect where a time-varying Doppler frequency provides the smearing mechanism. For target identifying applications, the registration-restoration-fusion method has been developed to refocus the distorted ISAR images. This method has been applied to both the experimental and simulated ISAR data. Results demonstrate that the registration-restoration-fusion motion compensation approach can improve the distorted ISAR image over what can be achieved by conventional Fourier transform methods. This study also adds insight into the distortion mechanisms that affect the ISAR images of a target in motion.**

I. Introduction

Inverse synthetic aperture radar (ISAR) imaging is an effective way to acquire high resolution images of targets of interest at long range and as such is an irreplaceable tool in the task of non-cooperative target recognition (NCTR) of both ships and aircraft [1]- [3]. The inverse synthetic aperture radar (ISAR) has attracted wide interest within scientific and military community. ISAR provides a 2-dimensional radar image of a moving target. Since ISAR imaging relies on the target's own motion, small random fluctuations in the target's motion can introduce severe distortion to the ISAR images. For example, small time-varying perturbed pitch, yaw or roll motion from fast maneuvering aircraft or ship can lead to smearing in the images. In real-world ISAR imaging scenarios, the target is often engaged in complicated maneuvers that combine translational and rotational motion. Unless a good motion compensation method is implemented, significant distortion can result in the ISAR image [2]- [5].

The distortion in the ISAR image of a target is a result of nonuniform rotational motion of the target during the imaging period. In many of the measured ISAR images from moving targets, such as those from in-flight aircraft, the distortion can be quite severe. Often, the image integration time is only a few seconds in duration and the targets' rotational displacement is only a few degrees.

Some ISAR applications are already well known and studied. However, many important issues remain to be addressed. For example, suitable enhancement techniques for the fast maneuvering radar targets or targets with fast moving parts is not yet known. Also, the standard approaches based on the Fourier transform (FT) fail to resolve the influence of closely spaced reflectors. There are several techniques for improvement of the ISAR radar image in the case of fast maneuvering targets or in the case of objects with complex reflector geometry. Here we mention only three groups of such enhancement techniques: (1) techniques that adapt transform parameters for assumed parametric target motion model [2]- [3]; (2) techniques that are based on time-frequency analysis methods [4]- [5]; and techniques where reflection signal components are parametrized, while the signal components caused by reflectors are estimated by using some of the well developed parametric spectral estimation tools [6]- [7].

IET Signal Processing, Vol. 2, No. 3, Aug. 2008.

All of these techniques have some advantages, but they also have some drawbacks for specific applications. The first group of techniques is strongly based on the radar target geometry with an assumed motion model. These techniques could become inaccurate in the case of a changing motion model. The second group of time-frequency techniques are known to be successful in refocusing blurred ISAR images. This occurs because the images are obtained at a particular instant in time when the target's motion can be considered as relatively uniform over the short duration. However there will be a large number of time instants to deal with time-frequency processing. Thus, a large number of refocused ISAR images will be generated, spanning the entire coherent integration time. For accurate target recognition, it is imperative to make use of only the best refocused image. It would be sometimes impractical and inefficient to examine all of the images produced in order to identify which is the best [8]. The third group of techniques is tested on simulated examples. However, its application in real scenarios, where signal components are caused by numerous scatterers, could be very difficult. Namely, there are no appropriate methods for parameter estimation of signals with a very large number of components.

In this paper we propose a modification of the first group of research techniques. A new approach is proposed to perform target translational and rotational motion non-uniformity compensation for ISAR imaging. The approach is based on a registration-restoration-fusion technique. It is important to note that the proposed technique does not assume any particular model of radar target motion. The adaptive parameters are estimated for each scattering point independently. The approach is based on a registration-restoration-fusion technique. Results demonstrate that this approach can be used as one of the ISAR refocusing procedures. Another contribution of this paper is that although several studies have been performed in image processing using the registration-restoration-fusion approach, this paper introduces this approach to ISAR imaging. As such, this paper contributes by presenting a new approach to focus distorted ISAR images and analysis which should add in developing a better picture of the motion compensation in ISAR imaging. The proposed approach has been successfully applied to both experimental and simulated ISAR data.

The paper is organized as follows. A brief analytic continuous-wave (CW) radar model is given in Section 2. Section 3 describes the Fourier transform used in ISAR imaging and its spreading terms that degrades the ISAR imaging. The registration-restoration-fusion motion compensation procedure is given in Section 4. Results and conclusions are given in Sections 5 and 6, respectively.

II. Analytic CW Radar Signal Model

For the analytic derivation of the model, consider a continuous wave (CW) radar that transmits a signal in the form of a coherent series of chirps [4]:

$$v_p(t) = \begin{cases} e^{(j\pi B f_r t^2)} & \text{for} \quad 0 \le t \le T_r \\ 0 & \text{otherwise} \end{cases} \qquad (1)$$

where T_r is the repetition time, $f_r = 1/T_r$ is the repetition frequency, and B is the emitted waveform bandwidth.

In one revisit, the transmitted signal consists of M such chirps:

$$v(t) = e^{(-j\omega_0 t)} \sum_{m=0}^{M-1} v_p(t - mT_r) \qquad (2)$$

where ω_0 is the radar operating frequency. The total signal duration is $T_c = MT_r$ and represents the coherent integration time (CIT).

Consider a signal of form (2) transmitted toward a target. If the target distance from the radar is d (referred to as range), then the received signal is delayed with respect to the transmitted signal for $t_d = 2d/c$, where c is the velocity of propagation, equal to the speed of light. The phase of the received signal is changed as $\phi = 2kd = 4\pi d/\lambda = 4\pi d f_0/c = 2\omega_0 d/c$.

Thus, the form of the received signal is

$$u(t) = \sigma e^{(j[-\omega_0(t-\frac{2d}{c})])} \sum_{m=0}^{M-1} v_p(t - \frac{2d}{c} - mT_r)$$

where σ is the reflection coefficient. The received signal is mixed (multiplied) with the complex-conjugate of the transmitted signal and shifted in time with a minimal delay T_0. We will assume that a constant distance is properly compensated and that $T_0 = 0$. Without loss of generality, we can consider only one component of the received signal:

$$q(m,t) = \sigma e^{(j\omega_0 \frac{2d}{c})} e^{(-j2\pi B f_r (t - mT_r)\frac{2d}{c})}.$$

A two-dimensional discrete signal is obtained by sampling in time with $t - mT_r = nT_s$

$$q(m,n) = \sigma e^{(j\omega_0 \frac{2d}{c})} e^{(-j2\pi B f_r n T_s \frac{2d}{c})}.$$

III. Fourier Transform in ISAR

The two-dimensional (2D) Fourier transform of the received signal is

$$Q(m',n') = \sum_{m=0}^{M-1} \sum_{n=0}^{N-1} q(m,n)$$
$$e^{(-j[2\pi m m'/M + 2\pi n n'/N])}$$

where time is discretized such that $t - mT_r = nT_s$. The periodiogram

$$P(m',n') = |Q(m',n')|^2$$

represents an ISAR image.

In order to analyze cross-range nonstationarities in the Fourier transform, we consider only the Doppler component part of the received signal (the p-th point scatterer), as it is usually done in the literature on ISAR,

$$\begin{aligned} e_p(t) &= \sigma_p e^{(j\frac{2\omega_0}{c} d_p(t))} \qquad (3) \\ &= \sigma_p e^{\left(j\frac{2\omega_0}{c}(x_p \cos(\theta_R(t)) + y_p \sin(\theta_R(t)))\right)}. \end{aligned}$$

The Fourier transform of $e_p(t)$ produces

$$E_p(\omega) = \int_{-Tc/2}^{T_c/2} e_p(t) e^{(-j\omega t)} dt$$

$$= \int_{-\infty}^{\infty} w(t) e_p(t) e^{(-j\omega t)} dt,$$

where $w(t)$ is the window defining the considered time interval. In order to simplify the notation we will omit the index p.

For time-varying $d(t)$, we can write a Taylor series expansion of $d(t)$ around $t = 0$:

$$\begin{aligned} d(t) &= d_0 + d'(0)t + \frac{1}{2} d''(0) t^2 + ... \qquad (4) \\ &= \sum_{n=0}^{\infty} \frac{1}{n!} d^{(n)}(0) t^n, \end{aligned}$$

where $d^{(n)}(0)$ is the $n-$th derivative of the distance at $t = 0$ and $2\omega_0 d'(0)/c = \Delta\omega_d$.

Fourier transform (FT) of (3) with (4) is of the form

$$E(\omega) = \int_{-\infty}^{\infty} w(t) e^{(j\frac{2\omega_0}{c} \sum_{n=0}^{\infty} \frac{1}{n!} d^{(n)}(0) t^n)} e^{(-j\omega t)} dt$$

$$= \int_{-\infty}^{\infty} w(t) e^{\left(j\frac{2\omega_0}{c}\left\{[d(0) + d'(0)t + \sum_{n=2}^{\infty} \frac{1}{n!} d^{(n)}(0) t^n\right\}\right)}$$
$$\times e^{(-j\omega t)} dt \qquad (5)$$

By omitting the constant term $d(0)$ and shifting $2\omega_0 d'(0)/c = \Delta\omega_d$ into the second exponential term we get

$$E(\omega) = \int_{-\infty}^{\infty} w(t) e^{(j\frac{2\omega_0}{c} \sum_{n=2}^{\infty} \frac{1}{n!} d^{(n)}(0) t^n)}$$
$$\times e^{(-j[\omega - 2\omega_0 d'(0)/c]t)} dt. \qquad (6)$$

This is a Fourier transform of a product of the window $w(t)$ and the first exponential function, calculated at the frequency $\omega - 2\omega_0 d'(0)/c = \omega - \Delta\omega_d$. The Fourier transform of a product of two functions is equal to the convolution of their Fourier transforms, resulting in

$$E(\omega) =$$
$$W(\omega - \Delta\omega_d) *_\omega FT\left[e^{(j\frac{2\omega_0}{c} \sum_{n=2}^{\infty} \frac{1}{n!} d^{(n)}(0) t^n)}\right],$$

where $*_\omega$ denotes convolution in frequency. Thus, the Fourier transform is located at and around the Doppler shift $\omega = \Delta\omega_d$. It is spread by the factor

$$S_{spread}(\omega) = FT\left[e^{(j\frac{2\omega_0}{c} \sum_{n=2}^{\infty} \frac{1}{n!} d^{(n)}(0) t^n)}\right].$$

This factor depends on the derivatives of the distance, starting from the second order (first order derivative of the Doppler shift), i.e., the spread factor depends on

$$s_f(t) = \frac{1}{2}d^{''}(0)t^2 + \frac{1}{6}d'''(0)t^3 + ...$$

It can significantly degrade the periodogram image:

$$P(\omega) = |E(\omega)|^2 .$$

This means that in the Fourier transform based image the spreading terms started from the second derivative $d^{''}(0)$. The goal of the ISAR signal processing is to obtain the focused radar image, i.e., to remove the influence of the second and higher terms in signal phase of each component.

IV. Registration-Restoration-Fusion Motion Compensation Procedure

The image registration, restoration and fusion are the basic image processing operations in remote sensing. A recorded image is likely to be degraded by sensor sampling. The purpose of this kind of image processing technique is to operate on the degraded image to obtain an improved image. Since it is similar to ISAR motion compensation, we developed a registration-restoration-fusion technique that is suitable for ISAR motion compensation and integrated them in one toolbox to make this motion compensation operation flexible and convenient. The motion compensation process includes three main steps: registration, restoration, and fusion [9]- [10].

The image registration is the process of matching two images (reference and input images) so that corresponding coordinate points in the two images refer to the same physical region of the scene being imaged. The accurate sub-pixel registration between two ISAR imaging frames is key to the success of automatic motion compensation. To perform point scatter automatic registration, a method named the 'nearest neighbor method' is developed to search for corresponding control points from two candidate images [9]- [10]. The method is to set a window around the position of a point scatterer that is found in the reference image. The position of point scatterers in the input image is determined on the chosen window. The registration parameters (scale and rotation angle) can be determined by the position relationship of two sets of control points. Then the registration methods, including the second, third, and fourth order polynomial methods, the linear conformal method, the affine method, and the projective and piecewise linear methods, are investigated and compared to generate the registered image [9]- [10]. A minimum number of control points are needed for these registration methods. The minimum number of point scatterers needed is equal to the number of registration parameters. If polynomial approximations are employed the number of registration parameters is increassed to include the parameters of the polynomial as well, which deal with spatial distortions.

A. Registration

Image registration is necessary to form a pixel-by-pixel comparison of two images. The problem of image registration is to determine the location at which a sub-image of a larger image is most similar to a given smaller image. To form this comparison, it is necessary to spatially register the images, and thereby, correct relative translation shifts, rotational differences, scale differences, and even perspective view differences. Often, it is possible to eliminate or minimize many of these sources of mis-registration by proper static calibration of an image sensor. However, in many cases, a posterior mis-registration detection and subsequent correction must be performed. A registration methodology generally consists of the following processes [11]- [16]: a) Identification of points in both images that corresponds to the same physical location on the field of view; b) Estimation of the registration parameters (nine in general, i.e., three rotations, three translations and three scaling); c) Modeling and correcting image sampling non-linearities (e.g. polynomial approximation methods); and d) Transforming of one image through affine transformations, interpolation and other supplementary 3-D information (e.g., DEM (Digital Elevation Models), if

available).

The most difficult step of image registration is the accurate identification of match points. The traditional approach uses human assistance to identify these points. Automated methods follow one of two main approaches [17]- [18]. Existing literature on image registration can be divided into two major categories, namely template matching and feature matching [11]- [16], [19]- [22]. In this paper, template matching was used for the image registration.

The distortions existed in the images may increase the difficulties and reduce accuracy of registration process. Sample distortion types include [23]: a) Sensor noise; b) Perspective changes from sensor viewpoint or platform perturbations; c) Object changes such as movements, deformations or growths; and d) Atmospheric scintillation effects.

B. Automatic Image Registration

The automatic ISAR image registration algorithm that is employed here has the following advantages over other techniques: a) It achieves sub-pixel accuracy in the mean-square-error sense; b) Employs a closed-form linear solution for the nine registration parameters; c) Uses enhanced local interpolation techniques; d) It is fully automatic. (It includes automatic control point estimation at high level of accuracy); e) Some of the available techniques achieve automatic registration for a certain range of the parameters. The developed approach does not set any constraints; and f) The developed approach is quite robust and works for different kinds image pairs.

Since the robustness and applicability to many types of imagery are important requirements, a template based matching technique is used to identify pairs of corresponding points in the images [19]- [22]. The template matching method takes advantage of information from all part of the image (rather than just at edges or other features), this is particularly important for the registration of noisy images. In the past, the correlation method was limited to the registration problems in which the images were misaligned by small rotational differences [24]- [25]. Many automatic registration programs only perform for small scaling and rotation factors. Our registration method has been used to deal with significant difference in image scaling and rotation factors. Our approach automatically finds scaling and rotation parameters between the two images, and then detects match points using both cross correlation and features extracted from the images. A consistency checking approach, that is a key for automatic registration process, is then performed to eliminate mismatched points. Then a three dimensional registration mapping function or other 2-D or 3-D high order mapping functions are computed and the second image is transformed and resampled to align with the first image. All processes are performed automatically without human assistance. Each step of the processes and its improvements are described herein.

B.1 Identifying the Match Points (Ground Control Points)

A set of match points (ground control points) is identified using the template matching technique. The template matching is followed by an Adaptive Weibull Constant False Alarm Rate (CFAR) detector to reduce the number of false positives [30]. The false alarm rate is determined by the user. In this experimental data, 10^{-6} was used for the CFAR. The first few identified match points are used to constrain the search area in the spatial domain. By relaxing the false alarm rate more points are identified. They define an increasingly accurate registration of the images, which predicts the locations of further match points. This method is similar to the multistage approach, but it does not require the images down sampling. Through quadratic interpolation of the correlation values of the template matching process, sub-pixel accuracy can be achieved. The number of match point pairs should be sufficient to result in an accurate mapping. Also, points in the first image are selected in a certain pattern in order to perform consistency checking in the following step [26].

Fast Fourier Transform (FFT) is used in the first two steps to accelerate the calculation of the cross-correlation. The first tem-

plate, $F_1(i,j)$, must be placed in an $M \times M$ pixel array and zero-padded to avoid end effects. Let $f_1(a,b)$ and $f_2(a,b)$ denote the two-dimensional Fourier transforms of $F_1(i,j)$ and $F_2(i,j)$,respectively. Then the cross-correlation function could be written as:

$$R(m,n) = IFFT[f_1 f_2^*(a,b)] \tag{7}$$

where * denotes the complex conjugate.

B.2 Consistency Checking

Due to distortion and changes between two images, small spatial mismatching errors may occur at the stage where the correspondence of the control points is assigned. The consistency matching process supports the automatic exclusion of false control points which are normally points with large spatial mismatching errors [27]. Hence, after all match points are obtained from the CFAR detector, we use position consistency checking as a constraint to reinforce the registration condition.

The consistency checking is applied using the nearest neighbor approach on a second order polynomial (i.e. for target-velocity-acceleration) [[27]]. Bounds on maximum velocity and acceleration may further reduce or eliminate mismatching points if the happen to occur at the neighbourhood of potential correct control points. It is very efficient in removing all mismatched points caused by image local distortion, changes between images, etc.

B.3 Finding the Scaling and Rotation Parameters

In general, the correlation methods were limited to image pairs with small rotational differences and no scaling differences. We have developed a solution to find matching points of two images with significant scaling and rotation differences. In most applications, the registration parameters are not known in advance. The first step in our registration process is to find those scaling and rotation parameters. We solve this problem by first correcting the template of the reference image. A modified matched filter is used to provide an output measure of the spatial correlation between the two images. A circular template is selected to cooperate with rotation problems. This circular template is then scaled and/or rotated with different values to match with the second image. This operation uses a nine-parameter transformation function for rotation and scaling. It should be noted that a fixed window size is used for the transformed template. The peak of cross correlation of different scaling and rotation values determines correct scaling and rotation parameters between the two images in the spatial domain. Although the scaling and rotation factors are not highly accurate, they can be used at next step to find accurate ground control points matching and be refined in the following step. A more accurate transformation between the two images is then obtained from all correctly matched ground control points.

Computation of the Registration-Mapping Function

A three-dimensional nine parameter model of rotation, translation and scaling (RTS) is used to calculate the registration-mapping function in the first step of the registration. The template mask is transformed using this function to deal with significant rotation and scaling. A least square method is used to solve the transformation parameters in Equation (9).

In our registration algorithm, the registration mapping function can be written as:

$$\begin{aligned}(x_1, y_1, z_1) &= F(x_2, y_2, z_2) = \\ &= A(x_2, y_2, z_2) + B(x_2, y_2, z_2)\end{aligned} \tag{8}$$

where B is a function that compensates image topographic heights of three-dimensional image registration. Detailed description of the B is not the focus of this research. A is a nine parameters model for affine transformation. It can be written in the following form:

$$\begin{aligned}&A(x_2, y_2, z_2) = \\ &= T \begin{bmatrix} x_{12} \ldots x_{N2} \\ y_{12} \ldots y_{N2} \\ z_{12} \ldots z_{N2} \\ 1 \ldots 1 \end{bmatrix} = \begin{bmatrix} x_{11} \ldots x_{N1} \\ y_{11} \ldots y_{N1} \\ z_{11} \ldots z_{N1} \\ 1 \ldots 1 \end{bmatrix}\end{aligned} \tag{9}$$

where T is the first order polynomial or the affine transformation matrix:

$$T = \begin{bmatrix} s_1\cos(\omega)\cos(\theta) & -s_2\cos(\omega)\sin(\theta) & -s_3\sin(\omega)\cos(\theta) & s_1 dx \\ -s_1\sin(\varphi)\sin(\omega)\cos(\theta)+s_1\cos(\varphi)\sin(\theta) & s_2\sin(\varphi)\sin(\omega)\sin(\theta)+s_2\cos(\varphi)\cos(\theta) & -s_3\sin\varphi\cos\omega & s_2 dy \\ s_1\cos(\varphi)\sin(\omega)\cos(\theta)+s_1\sin(\varphi)\sin(\theta) & -s_2\cos(\varphi)\sin(\omega)\sin(\theta)+s_2\sin(\varphi)\cos(\theta) & s_3\cos\varphi\cos\omega & s_3 dz \\ 0 & 0 & 0 & 1 \end{bmatrix} \tag{10}$$

where s_1, s_2 and s_3 are scaling parameters in three dimensions; φ, ω and θ are rotation angles around the x, y and z-axis respectively; dx, dy and dz are translation parameters in the three axes respectively. A least square method is used to solve these transformation parameters.

Equation (10) may be written as follows:

$$T\,X = Y$$

and the least squares solution with respect to T is

$$T = Y\,X'[X\,X']^{-1}$$

The parameters vector [θ,φ, ω, s_1, s_2, s_3, dx, dy, dz] found directly from the entries of the matrix T, and although the relationships look nonlinear, these parameters are uniquely defined through a direct (non iterative) solution, employing straightforward mathematical manipulations [28] (see also Appendix A).

We improve our previous linear model with Delaunay triangulation and a high order polynomial, non-linear model. Equation (11) is an example of second order model for two-dimensional image transformation with 12 parameters:

$$x_1 = a_1 + a_2x_2 + a_3y_2 + a_4x_2y_2 + a_5x_2^2 + a_6y_2^2$$

$$y_1 = b_1 + b_2x_2 + b_3y_2 + b_4x_2y_2 + b_5x_2^2 + b_6y_2^2 \tag{11}$$

For N matched pairs, the above equation can be written as:

$$\begin{bmatrix} x_{11} & y_{11} \\ x_{21} & y_{21} \\ . & . \\ . & . \\ . & . \\ x_{N1} & y_{N1} \end{bmatrix} = \begin{bmatrix} 1 & x_{12} & y_{12} & x_{12}y_{12} & x_{12}^2 & y_{12}^2 \\ 1 & x_{22} & y_{22} & x_{22}y_{22} & x_{22}^2 & y_{22}^2 \\ . & . & . & . & . & \\ . & . & . & . & . & \\ . & . & . & . & . & \\ 1 & x_{N2} & y_{N2} & x_{N2}y_{N2} & x_{N2}^2 & y_{N2}^2 \end{bmatrix} =$$

$$= \begin{bmatrix} a_1 & b_1 \\ a_2 & b_2 \\ . & . \\ . & . \\ . & . \\ a_6 & b_6 \end{bmatrix} \tag{12}$$

A least square method is used to solve this Equation (12). The affine transformation parameters can also be obtained.

B.4 Resampling and Transforming the Image

The second image is resampled and transformed to align with the first image. Available methods include nearest neighbor interpolation, bilinear interpolation, cubic spline interpolation, bicubic interpolation and quadratic interpolation. After the comparison among different interpolation methods, we have chosen the bilinear interpolation, which provided better results for our data sets.

B.5 Registration Accuracy

The registration accuracy is commonly measured by the root-mean-square (RMS) error between the matched points after the transformations have been applied:

$$RMS(N) = \left(\frac{1}{N} \sum_{i=1}^{N} \left\{ [x_{1i} - F_x(x_{2i}, y_{2i})]^2 + [y_{1i} - F_y(x_{2i}, y_{2i})]^2 \right\} \right)^{1/2} \tag{13}$$

If $RMS(N) < 1$, sub-pixel accuracy is achieved in the root-mean-square-error sense.

It should be noted that RMS error is calculated based on the correctly identified ground control points. It relies on i) the number of

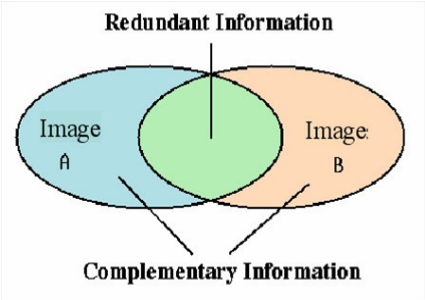

Fig. 1. The concept of image fusion

points used in the calculation ii) the distribution of the points iii) the transformation function F_x and F_y used between the two images. A small RMS error means that error between the registered images is usually small (at least around those ground control points). If the images have distortions from the transformation function, the errors at the distortion areas usually are larger than other image areas. If the image scenes can be perfectly modeled by a transformation function (no distortion), the RMS error will provide a good indication of the registration accuracy for the whole image scene. Based on our results from our testing on multiple image registration, with the approach described above, images are automatically registered at sub-pixel accuracy.

C. Restoration and Fusion

The blur estimation is a key step for image restoration. It takes an image that has been degraded by linear blur, which is an image that has been convolved with some point-spread function (PSF), and returns an estimate of the original image [29]- [30]. The PSF can be specified as a mask whose dimensions are smaller than those of the image, or it can be specified as a mask whose dimensions are identical to those of the image. Our in-house toolbox provides blur estimation, which can be accessed from the restoration toolbox interface. If the blur function exists, it could be used in the restoration operation directly. The restoration process can be used after the registration process to reduce blur. It can also be used before the registration to separate two adjacent point scatterers in order to generate accurate motion parameters. Five restoration methods such as least squares restoration, resolution-to-noise trade-off restoration, Lucy-Richardson restoration, regularized filter algorithm, and Wiener filter algorithm have been investigated and compared [31]- [32]. In this paper, we have used Lucy-Richardson restoration, which provided better results for our data sets. Finally, the fusion process is applied to two or more registered ISAR images in order to improve the reliability and capability of target recognition [5]. The reason for this is that the fused image has more complete target information than the input images. The fused image is produced from two or more input images by utilizing redundant and complementary information as shown in Figure 1.

It should be emphasized here that several methods have been developed for registration, restoration, and fusion methods in the image processing. It is not the objective of this paper to perform trade-off studies of the individual methods. Rather, the objective is to demonstrate the proposed approach by using the experimental and simulated ISAR data and provide some insight as to how the registration-restoration-fusion approach can be used for focusing ISAR images. In this paper, we develop the preliminary ground work for this challenging field of research.

V. Results

We demonstrate the application and effectiveness of the registration-restoration-fusion motion compensation procedure with three simulated data sets and six measured experimental radar data sets.

A. Simulated Data

To gain a better physical insight into the scattering phenomenon of an aircraft's ISAR image, an aircraft can be assumed to be composed of a set of point scatterers on a two-dimensional plane. Each scattering point on the aircraft does not represent any geometric point on the target but a combination of scattering sources that return a radar echo. A two-dimensional model of an aircraft's scattering centers is sufficiently adequate to analyze the ISAR images of aircraft. In this simulation we assume the target contains six microwave corner reflectors (i.e., scatterers) to simulate the distorting effect that could occur in ISAR images.

The center frequency of the radar is 9 GHz and the bandwidth is 300 MHz. A total of 30 range cells and 50 cross-range cells are used for the imaging. In Figure 2a, we show the image from the simulated data without any added motion error as a reference for comparison. This figure illustrates the undistorted ISAR image when the target is uniformly rotating at a constant rate of 3 degrees/second. Since there are no random motions, we can use the conventional Fourier transform; that is, we take a series of one-dimensional Fourier transforms across the target. As expected, the image is well-focused.

Then we inject perturbed random motion (or motion error) into the simulation. That is, in addition to the uniform (3 degrees/second) rotation we inject perturbed random motion through a 'sine-drive' by adding an additional sine wave to the motion. The resultant rotational motion will then be a non-uniform. It should be noted here that the rotational motion of the target is confined to a two-dimensional plane during the coherent processing interval. Figure 2b illustrates the distorted image obtained by using the conventional Fourier transform. In this case, the perturbed oscillation is 1 Hz. The figure clearly shows that the image is severely distorted, which means that target itself contains much rotational error. The image is smeared along the cross-range direction. This is because of the target's complex motion due to perturbed random motion during the entire coherent processing interval. The conventional radar imaging that uses Fourier transform, which works well for uniform rotational motion, cannot be directly applied to the perturbed target. The registration-restoration-fusion algorithm is then applied to this data. Figure 2c illustrates the final image after the registration, restoration, and fusion procedures. All the scatterers are well focused in their individual range and cross-range cells. This implies that all the quadratic phase terms are eliminated. In Figure 2d, we show another image from the simulated data without any added motion error. The orientation of the target is different from the previous example. Figure 2e illustrates another example of a distorted image due to perturbed random motion error. The image is poorly focused and the image of each scatterer is severely smeared. In this case, the perturbed oscillation is 0.75 Hz. Figures 2f shows that the registration-restoration-fusion motion compensation algorithm successfully eliminates the quadratic phase terms and shows a well-focused ISAR image. In Figure 2d, the image from the simulated data without any added motion errors is shown as a reference for comparison. We can see that the motion-compensated image achieves the same sharpness as the reference image.

Another example is a MiG-25 aircraft with 120 point-scatterers distributed along the edge of the 2D shape of the aircraft [4]. The simulation uses a stepped frequency X-band radar operating at a center frequency of 9 GHz. With a total of 64 stepped frequencies, it has a bandwidth of 512 MHz and a range resolution of 0.293 m. The pulse repetition frequency (PRF) is 20 kHz and the CIT is 1.64 seconds. A total of 64 range cells and 512 cross-range cells are used for the imaging. The aircraft is at a range of 3,500 m and is rotating at 10 degrees/second, thus giving a cross-range resolution of about 0.058 m. The rotation rate is much higher than the normal rotation rate needed to produce a clear image of the target. We assume that target's translational motion can be perfectly compensated. However, due to the fast rotation and relatively longer image observation time, even after standard motion compensation, the uncompen-

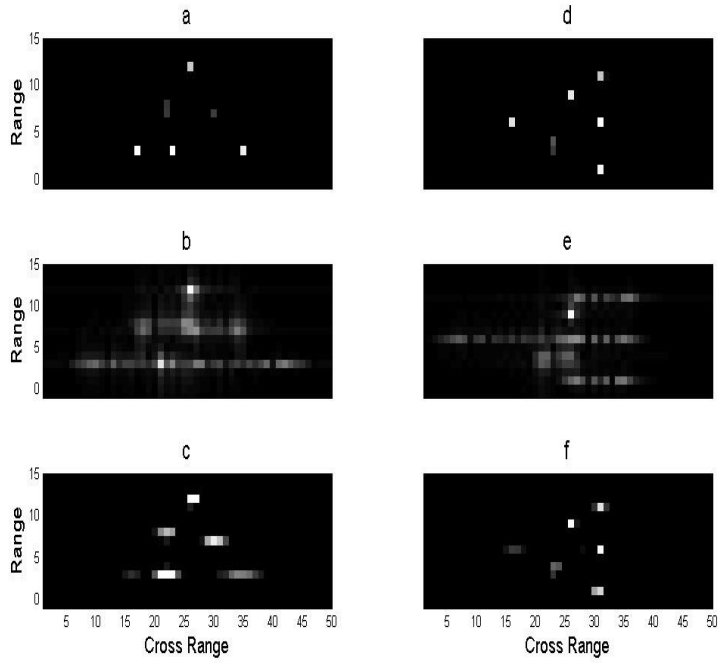

Fig. 2. (a) ISAR image using FT. The 6 reflectors are uniformly rotating at a constant rate of 3 degrees/second. The data has no random error. This image is used as a reference for comparison; (b) Distorted ISAR image using FT. The data has random motion error; (c) Focused ISAR image using the registration–restoration-fusion motion compensation algorithm. (d) Another simulated ISAR image without any added motion error; (e) Distorted ISAR image using FT. The data has random motion error; (f) Focused ISAR image using the registration–restoration-fusion motion compensation algorithm.

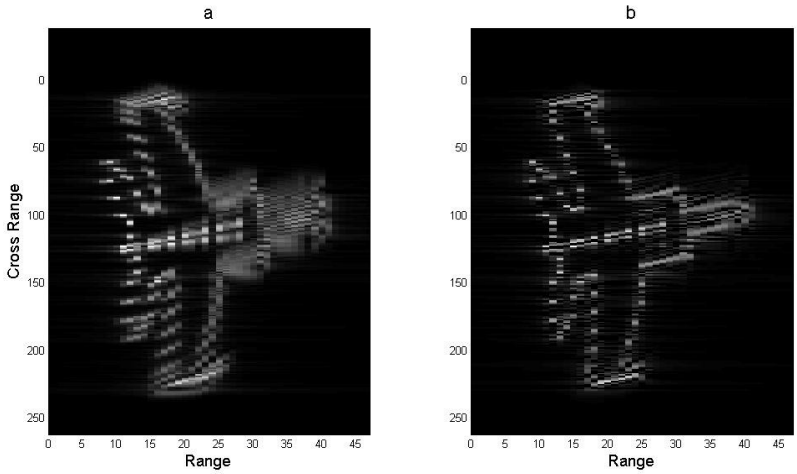

Fig. 3. (a) FT-based ISAR image formation and (b) Registration-restoration-fusion based ISAR image formation.

sated phase error is still large. The FT-based image of the radar target is depicted in Figure 3a. The radar image obtained by using the registration-restoration-fusion approach is presented in Figure 3b. These results suggest that improvement of the radar image can be achieved by using the registration-restoration-fusion motion compensation approach.

B. Experimental Data

An ISAR experiment is set up to examine the distortion in ISAR images due to a time-varying rotational motion. There are a number of reasons why data from a controlled experiment are desirable. In a controlled experiment, the locations of the scattering centres and the rotational axis of the target are known precisely. The rotational motion of the target can be programmed and controlled to produce the desired effects that are sought for analysis. Moreover, experiments of a given set of conditions can be repeated to verify the consistency of the results. These are not always possible with real targets such as in-flight aircraft. Data from controlled experiments can then be used to compare with simulated results from the numerical models under the same set of conditions. Such comparisons provides a meaningful validation of the numerical model, thus proving a clearer picture of the distortion process. Controlled experiments allow us to set the desired rotation rate and then permit us to cross check and assess the results.

A target motion simulator (TMS), a 2-dimensional delta-wing, is designed and built, allowing the study of the distortion effect in ISAR images under controlled experimental conditions. A picture of the TMS is shown in Figure 4. The experimental apparatus enables us to simulate a small time-varying fluctuating motion on the target. It allows us to conduct controlled experiments where the rotational rate and the fluctuating motion of the target can be pre-determined. One of the objectives of this paper is to demonstrate that gross distortion can occur in the target's ISAR image as a result of small fluctuating motion. In this experiment, the target has a length of 5 m on each of its three sides. Six trihedral reflectors are mounted on the TMS as scattering centres of the target; all the scatterers are located on the x-y plane. They are designed to always face towards the radar as the TMS rotates. The TMS target is set up so that it rotates perpendicular to the radar line of sight. This simplified target geometry is identical to the one used in the numerical model given in the previous section. Note that one corner reflector is placed asymmetrically to provide a relative geometric reference of the TMS target. A time-varying rotational motion is introduced by a programmable motor drive. The delta-wing data was collected using an X-band radar operating at a center frequency of 10.1 GHz with 300 MHz bandwidth and a range resolution of 0.5 m. The PRF is 2 kHz. Each HRR profile is generated in 0.5 ms and each profile has 41 range bins. The total data set contains 60,000 HRR profiles. The delta-wing is at a range of 2 km and initially rotating at 1.4 degrees/second for about 10 seconds. Then, an oscillating motion at about 1 Hz is superimposed onto to the constant motion. After 10 seconds, the rotation rate is gradually increased to 2 degrees/second. Since the TMS stationary, i.e., no radial translation motion along the radar's line-of-sight and subsequently no range alignment between HHR profiles in the down range direction is needed in forming the ISAR images. The only adjustment required is the centering of the HRR profiles in the down range direction such that the processed ISAR image is centered in the viewing window.

According to the principles of ISAR imaging, a long image integration time is required to produce fine image resolution. However, a long image integration time does not always guarantee good cross-range resolution. This will also be illustrated in this section. Since the entire data set consists of 60,000 pulses in the cross-range, it can be "cut" into different size imaging intervals with each of the intervals displaying a different amount of motion error. This is the approach used in this paper. The proposed method in now applied for three different imaging intervals, i.e., 2, 3, and 4 seconds of duration. The image at the time of the first, second, and third second are taken to demonstrate the registration-restoration-

Fig. 4. Picture of the delta-wing target motion simulator apparatus.

TABLE I
THE POSITION OF POINT SCATTERER IN THE REFERENCE IMAGE, INPUT IMAGE AND REGISTERED IMAGE.

Reference Image (Base Points)	Input Image (Input Points)	Registered Image S-method
25 11	24 9	25 11
17 24	17 26	17 24
26 21	26 20	26 21
27 30	27 31	27 30
23 29	23 29	23 29
21 18	21 18	21 18

TABLE II
THE POSITION OF POINT SCATTERER IN THE REFERENCE IMAGE, INPUT IMAGE AND REGISTERED IMAGE.

Reference Image (Base Points)	Input Image (Input Points)	Registered Image S-method
25 24	25 26	25 24
28 23	28 24	28 23
25 20	25 19	25 20
20 21	20 21	20 21
21 18	21 16	21 18
19 25	19 27	19 25

fusion motion compensation process. The results are shown in Figure 5. In this figure, the image at the time of the first second in Figure 5a is a reference image. The image at the time of the third second in Figure 5b is the input image and will be registered to the reference image. The image Figure 5c is the registration result. The corresponding positions of control points and the positions of point scatterers of the registered image are shown in Table 1. The fused image is shown in Figure 5d, which corresponds to the integration time of 3 seconds. Figure 6 shows the results of a second example corresponding to the 12th and the 13th second of the data. The 12th second image in Figure 6a is considered as the reference image, and the 13th second image in Figure 6b is the input image that is registered to the reference image. The result is shown in Figure 6c, the corresponding positions of the point scatterers are shown in Table 2. The processing also gives good performance. The fused image is shown in Figure 6d, which corresponds to the integration time of 2 seconds. This image is more

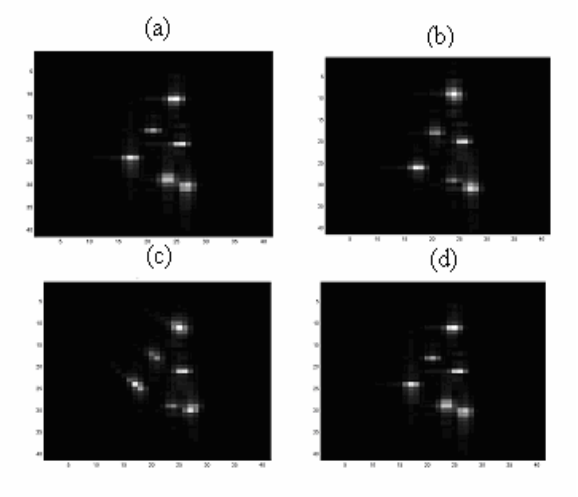

Fig. 5. The results from frame 1 and 3 of real data. (a) Reference image; (b) input image; (c) registered image; (4) fused image.

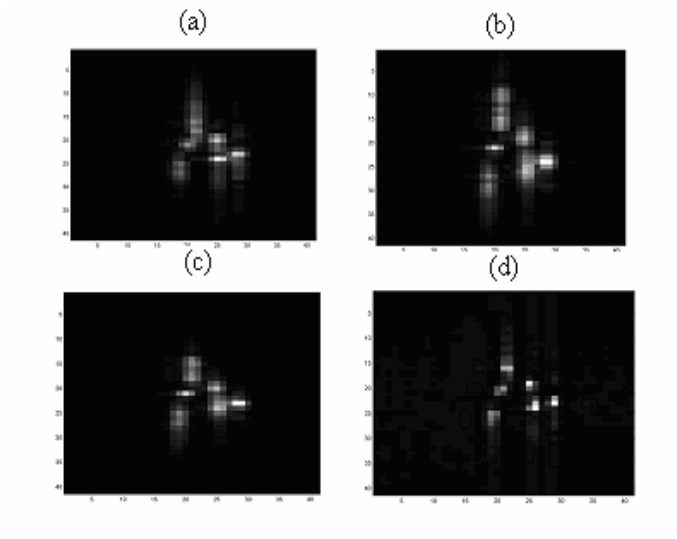

Fig. 6. The results from frame 12 and 13 of real data. (a) Reference image; (b) input image; (c) registered image; (4) fused image.

focused than the original image. These results indicate that the registration-restoration-fusion motion compensation approach is able to produce focused images.

Four different data sets are analyzed to further demonstrate the proposed method. Two ISAR images, one with an integration time of 2 seconds (Figure 7) and the other one with an integration time of 4 seconds (Figure 8), exhibit different amount of distortion. Figures 7-8 show ISAR images, which are analyzed when the rotation rate of the target attains 2 degrees/second. In these cases, the distortion of the ISAR images are severe than the previous examples (Figures 5 and 6). Figures 7a and 7b correspond to one data set and Figures 7c and 7d correspond to another data sets but with the same integration time

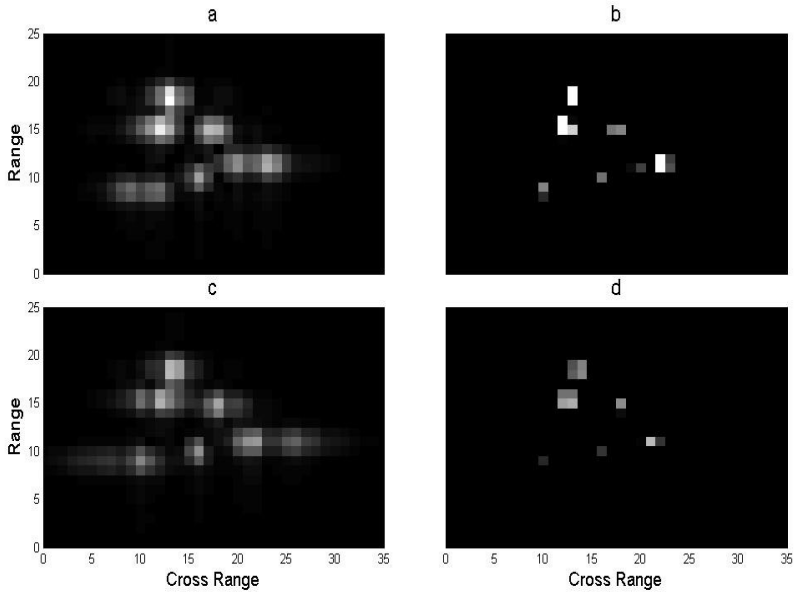

Fig. 7. Image integration period of 2 seconds: (a) Distorted ISAR image using FT; (b) Focused ISAR image using the registration–restoration-fusion motion compensation algorithm; (c) Another distorted ISAR image using FT; (b) Focused ISAR image using the registration–restoration-fusion motion compensation algorithm.

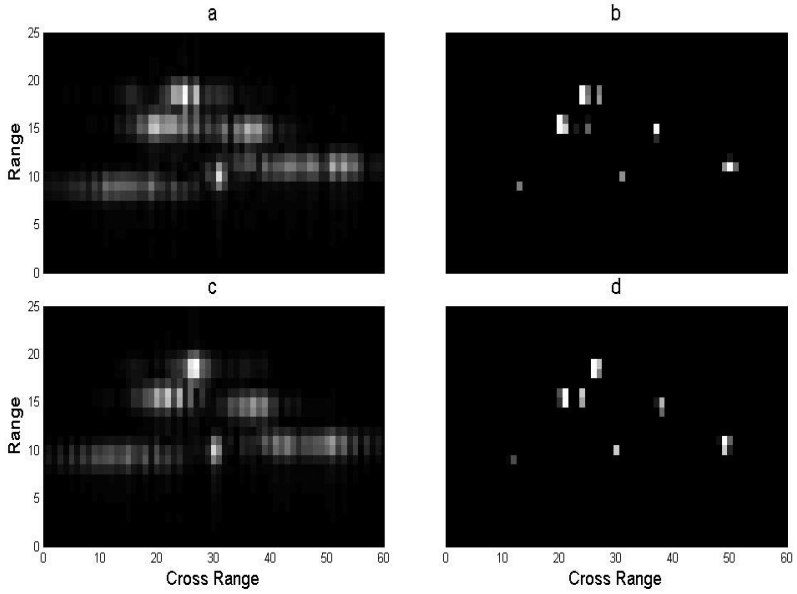

Fig. 8. Image integration period of 4 seconds: (a) Distorted ISAR image using FT; (b) Focused ISAR image using the registration–restoration-fusion motion compensation algorithm; (c) Another distorted ISAR image using FT; (b) Focused ISAR image using the registration–restoration-fusion motion compensation algorithm.

of 2 seconds. Similarly, Figures 8a and 8b correspond to one data set and Figures 8c and 8d correspond to another data sets but with the same the integration time of 4 seconds. Note that the 4-second ISAR image has two times higher cross-range resolution than the 2-second ISAR image. Results indicate that the registration-restoration-fusion motion compensation approach is able to produce focused images. These results are comparable with the results obtained from adaptive joint time-frequency method [3]. These results suggest that the registration-restoration-fusion approach provides a candidate to resolve the image smearing caused by the time-varying behavior and leads to a focused ISAR image. This topic remains for our future research.

We have also made the following observations from the experimental data. First, ISAR images with the same imaging time duration can have different amount of observation. This is illustrated in Figures 6 and 7. The two ISAR images both have a 2-second image integration time. But the decree of distortion is different in each image. Second, the distortion is directly related to the amount of change in the Doppler motion during the image integration period, which is illustrated in Figure 8. On the other hand, the distorted ISAR image processed using an image integration time of 3 seconds (Figure 5) has less amount of distortion as the distorted image using only 2-second of image integration time (Figures 6 and 7). This is because of the fluctuating motion that caused the change in the Doppler motion. It can be summarized that the distortion is dependent on the amount of maximum Doppler change within the image integration time.

VI. Conclusion

The experimental data offer clear evidence that the ISAR images can suffer large distortion when the target is subject to a small time-varying perturbed motion during the image integration period. The large distortion is attributed to the modulation effect in the phase of the radar return of a target with fluctuating motion. This results in blurring in the cross-range direction of the ISAR image due to a time-varying Doppler velocity from the fluctuating motion. In essence, the fluctuating target motion introduces a non-linear effect in the phase of the radar signal, resulting in the distortion of the ISAR image. The size of distortion is determined by the amount of variation in the Doppler motion occurred during the imaging duration and is independent of the length of the image integration time.

For target recognition applications, the blurred ISAR images of a moving target must be refocused to provide usable images for identification. An ISAR refocusing procedure was developed in this paper. A motion compensation method based on a registration-restoration-fusion approach has been proposed to perform ISAR motion compensation. The registration-restoration-fusion motion compensation technique has been applied to both the simulated and measured experimental ISAR data sets. The results demonstrate that the registration-restoration-fusion motion compensation approach gives good performance and generates focused ISAR images. In all cases, while the Fourier transform produced images with severe blurring, the registration-restoration-fusion motion compensation approach was able to produce focused images of the targets. Results indicate that the registration-restoration-fusion motion compensation approach outperforms the conventional Fourier transform method in improving blurred and distorted ISAR images due to various target motions. These results are comparable to the results obtained from adaptive joint time-frequency method [3]. The registration-restoration-fusion approach can be used as an alternative method for radar imaging but this topic remains for our future research.

Appendix A

As discussed in Section 3.24, Equation (19) can be written as follows:

$$T\,X = Y$$

and the least squares solution with respect to T is

$$T = Y\,X'[X\,X']^{-1}$$

The matrix T is a 4×4 matrix as described in Equation (10). The matrix T can be written as follows:

$$T = \begin{bmatrix} t_{11} & t_{12} & t_{13} & t_{14} \\ t_{21} & t_{22} & t_{23} & t_{24} \\ t_{31} & t_{32} & t_{33} & t_{34} \\ 0 & 0 & 0 & 1 \end{bmatrix}$$

where

$$\begin{aligned}
t_{11} &= s_1 \cos(\omega)\cos(\theta) \\
t_{12} &= -s_2 \cos(\omega)\sin(\theta) \\
t_{13} &= -s_3 \sin(\omega)\cos(\theta) \\
t_{14} &= s_1 dx \\
t_{21} &= -s_1 \sin(\varphi)\sin(\omega)\cos(\theta) + s_1 \cos(\varphi)\sin(\theta) \\
t_{22} &= s_2 \sin(\varphi)\sin(\omega)\sin(\theta) + s_2 \cos(\varphi)\cos(\theta) \\
t_{23} &= -s_3 \sin\varphi \cos\omega \\
t_{24} &= s_2 dy \\
t_{31} &= s_1 \cos(\varphi)\sin(\omega)\cos(\theta) + s_1 \sin(\varphi)\sin(\theta) \\
t_{32} &= -s_2 \cos(\varphi)\sin(\omega)\sin(\theta) + s_2 \sin(\varphi)\cos(\theta) \\
t_{33} &= s_3 \cos\varphi \cos\omega \\
t_{34} &= s_3 dz
\end{aligned}$$

The values of the parameters [θ,φ, ω, s_1, s_2, s_3, dx, dy, dz] are obtained by applying the following equations in the order that they are presented below.

a) The rotation around the x-axis:

$$\varphi = \tan^{-1}\left(\frac{t_{23}}{t_{33}}\right)$$

b) The rotation around the y-axis:

$$\omega = \tan^{-1}\left(\frac{t_{23}}{t_{13}}\right)\sin\varphi$$

c) The z-scaling parameter s_3 is given by

$$s_3 = \frac{t_{33}}{\cos(\varphi)\cos(\omega)} \text{ or}$$

$$= \frac{-t_{13}}{\sin(\omega)} \text{ or}$$

$$s_3 = \frac{-t_{23}}{\sin(\varphi)\cos(\omega)}$$

d) The translation parameter dz is given by

$$dz = \frac{t_{34}}{s_3}$$

e) The rotation parameter around the z-axis in given by

$$\theta = \tan^{-1}\left[\frac{\frac{t_{21}}{t_{11}} + \frac{\sin(\varphi)\sin(\omega)}{\cos(\omega)}}{\frac{\cos(\varphi)}{\cos(\omega)}}\right] \text{ or}$$

$$\theta = \tan^{-1}\left[\frac{\frac{-\cos(\varphi)}{\cos(\omega)}}{\frac{t_{22}}{t_{12}} + \frac{\sin(\varphi)\sin(\omega)}{\cos(\omega)}}\right] \text{ or}$$

$$\theta = \tan^{-1}\left[\frac{\frac{t_{31}}{t_{11}} - \frac{\cos(\varphi)\sin(\omega)}{\cos(\omega)}}{\frac{\sin(\varphi)}{\cos(\omega)}}\right] \text{ or}$$

$$\theta = \tan^{-1}\left[\frac{\frac{\sin(\varphi)}{\cos(\omega)}}{\frac{t_{32}}{t_{12}} + \frac{\cos(\varphi)\sin(\omega)}{\cos(\omega)}}\right]$$

f) The scaling parameter s_1 is given by

$$s_1 = \frac{t_{11}}{\cos(\omega)\cos(\theta)} \text{ or}$$

$$s_1 = \frac{-t_{21}}{-\sin(\varphi)\sin(\omega)\cos(\theta) + \cos(\varphi)\sin(\theta)} \text{ or}$$

$$s_1 = \frac{t_{31}}{\cos(\varphi)\sin(\omega)\cos(\theta) + \sin(\varphi)\sin(\theta)}$$

g) The translation parameter dx is given by

$$dx = \frac{t_{14}}{s_1}$$

h) The scaling parameter s_2 is given by

$$s_2 = \frac{t_{12}}{-\cos(\omega)\sin(\theta)} \text{ or}$$

$$s_2 = \frac{-t_{22}}{\sin(\varphi)\sin\omega\sin\theta + \cos(\varphi)\cos(\theta)} \text{ or}$$

$$s_2 = \frac{t_{32}}{-\cos(\varphi)\sin\omega\sin\theta + \sin(\varphi)\cos(\theta)}$$

i) The translation parameter dy is given by

$$dy = \frac{t_{24}}{s_2}$$

References

[1] C. C. Chen and H. C. Andrews, Target motion induced radar imaging, IEEE Trans. Aerosp. Electron. Syst., 16, pp. 2–14, 1980.

[2] Y. X. Wang, L. Hao, and Chen V. C., ISAR motion compensation via adaptive joint time-frequency technique, IEEE Trans. On Aerosp. Electron. Syst., vol. 34, No. 2, April 1998.

[3] T. Thayaparan, G. Lampropoulos, S.K. Wong and E. Riseborough, Application of an adaptive joint time-frequency algorithm for focusing distorted ISAR images from simulated and measured radar data, IEE Proceedings – Radar, Sonar and Navigation, Volume: 150, Issue: 4, Aug. 2003.

[4] V. C. Chen and H. Ling, Time-Frequency Transforms for Radar Imaging and Signal Analysis, Artech House, Boston, MA, USA, 2002.

[5] G. Lampropoulos, T. Thayaparan, and N. Xie, Fusion of Time Frequency Distributions and Applications to Radar Signals, Journal of Electronic Imaging, in press, 2006.

[6] S. Barbarossa, A. Scaglione, G. B. Giannakis: "Product high-order ambiguity function for multicomponent polynomial-phase signal modeling," *IEEE Trans. Sig. Proc.*, Vol. 46, No. 3, Mar. 1998, pp. 691-708.

[7] A. Quinquis, C. Ioana, E. Radoi: "Polynomial phase signal modeling using warping-based order reduction," in *Proc. of ICASSP'04*, Vol. 2, May 2004, pp. 741-744.

[8] Wong, S. K., Riseborough, E., and Duff, G. (2006). An analysis of ISAR image distortion based on the phase modulation effect, *EURASIP J. on appl. Sig. Processing,* pp. 1-16.

[9] B. Zitova and J. Flusser, Image registration methods: a survey, Image and Vision Computing, 21, pp. 977-1000, 2003.

[10] T. M. Lehmann, C. Gonner, and K. Spitzer, Survey: interpolation methods in medical image processing, IEEE Trans. on Medical Imaging, Vol. 18, No. 11, pp. 1049-1075, 1999.

[11] Barnea, D.J., and Silverman, H. F., A class of algorithms for fast digital image registration, IEEE Trans. on computers, vol. 21, 179-186, 1972.

[12] Davies, I. O. G., and Pedleg, M., Image Registration Algorithms, IEE colloquium on Applications of Motion Compensation (Degest No. 128), London, UK, 2/1-4, 1990.

[13] Goshtasby, A., Gage, S. H., and Bartholic, J. F., A two-stage cross correlation approach to template matching, IEEE Trans. on Pattern Analysis and Machine Intelligence, vol. 6, 374-378, 1984.

[14] Lampropoulos, G. A., Halet, A., Rey, M. and Boulter, J. F., E-O and SAR image analysis and registration applications, Proceedings of the 1997 SPIE Conference on Sensor Fusion: Architectures, Algorithms, and Applications, vol. 3067, 171-178, Orlando, Florida, U.S.A.

[15] Morandi, C., Piazza, F., and Dolcetti, A., Image registration using Fermat transforms, Electronics Letters, vol. 24, 678-679, 1988.

[16] Pratt, W. K., Digital Image Processing, A Wiley-Interscience Publication, 1991.

[17] Dhond, U. R., and Aggarwal, J. K., Structure from Stereo–A review, Int. J. Remote sensing, v.10, no. 6, 989, 1989.

[18] Hsieh, Y. C., Perlant, F., and McKeokn, D. M., Recovering 3D Information from Complex Aerial Imagery, Proc. of the 10th Int. Conf. on Pattern Recognition, v.1, III, Piscataway, NJ, 145, 1990.

[19] Li, X., and Dubes, R. C., The first stage in two-stage template matching, IEEE Trans. on Pattern Analysis and Machine Intelligence, vol. 7, 700-707, 1985.

[20] Rosenfeld, A., and Vanderburg, G. J., Coarse-fine template matching, IEEE Trans. on Systems, Man and Cybernetics, 104-107,1997.

[21] Rezaie, B., and Srinath, M. D., Algorithms for fast image registration, IEEE Trans. on Aerospace Electronics Systems, vol. 20, 716-727, 1984.

[22] Wessley, H. W., Image Correlation –Part II: Theoretical Basis. Report R-2057/2-PR, The rand Corporation, Santa Monica, California.

[23] L. G. Brown, A Survey of Image Registration Techniques. ACM Computing Surveys 23(1): 5 - 48 (1991). Volume 24, Number 4, December 1992.

[24] A.U.G. Sinals Ltd., 2000. Automatic image registration of satellite images from similar sensors and multiple sensors, Final Report IRAP # 321327.

[25] Zheng, Q., and Chellappa, R., A computational version approach to image registration, IEEE Trans. on Image Process, vol. 3, no. 3, 311-326, 1993.

[26] V. Anastassopoulos and G.A. Lampropoulos, "Optimal CFAR Detection in Weibull Clutter", IEEE Transactions on Aerospace and Electronic Systems, Volume 31, Issue No. 1, pp. 52-64, January 1995.

[27] G.A. Lampropoulos, J. Chan, J. Secker Y. Li, and A. Jouan, "Automatic registration of electro-optical and SAR images", Advances in Techniques for Analysis of Remotely Sensed Data, 2003 IEEE Workshop on; 27-28 Oct. 2003 Page(s):219 – 226.

[28] G.A. Lampropoulos, "Processing for Space-Based Electro-Optical Surveillance", Final Report No: R&D-0019/99, A.U.G. Signals Ltd. Contract from the Canadian Department of Defence, No: W7701-6-1637/001/XSK, May 1999.

[29] J. H. Elder and S. W. Zucker, Local scale control for edge detection and blur estimation, IEEE Trans. on Pattern and Analysis and Machine Intelligence, Vol. 20, No. 7, pp. 699-715, July 1998.

[30] Grinvald, A., Lieke, E. E., Frostig, R. D., and Hildesheim, R. (1994). Cortical point-spread function and long-range lateral interactions revealed by real-time optical imaging of macaque monkey primary visual cortex. Journal of Neuroscience, 14:2545– 2568.

[31] W. H. Richardson, "Bayesian-based iterative method of image restoration," J. Opt. Soc. Am., vol. 62, pp. 55–59, 1972.

[32] L. B. Lucy, "An iterative technique for the rectification of observed distributions," The Astronomical Journal, 79(6):745–754, 1974.